ACS APPLIED MATERIALS & INTERFACES

Research Article

www.acsami.org

Cellphone Camera Imaging of a Periodically Patterned Chip as a Potential Method for Point-of-Care Diagnostics

Ritu Gupta,[†] Ronald G. Reifenberger,*[,‡] and Giridhar U. Kulkarni*[,†]

[†]Chemistry and Physics of Materials Unit, DST Unit on Nanoscience, Jawaharlal Nehru Centre for Advanced Scientific Research, Jakkur P.O., Bangalore, Karnataka 560064, India

[‡]Birck Nanotechnology Center, Purdue University, West Lafayette, Indiana 47907, United States

Supporting Information

ABSTRACT: In this study, we demonstrate that a disposable chip periodically patterned with suitable ligands, an ordinary cellphone camera, and a simple pattern recognition software, can potentially be used for quantitative diagnostics. A key factor in this demonstration is the design of a calibration grid around the chip that, through a contrast transfer process, enables reliable analysis of the images collected under variable ambient lighting conditions. After exposure to a dispersion of amine terminated silica beads used as analyte mimicking pathogens, an epoxy-terminated glass substrate microcontact printed with octadecyltrichlorosilane (250 μm periodicity) developed a characteristic pattern of beads which could be easily imaged with a cellphone camera of 3.2 MP pixels. A simple pattern recognition algorithm using fast Fourier transform produced a quantitative estimate of the analyte concentration present in the test solution. In this method importantly, neither the chip fabrication process nor the fill-factor of the periodic pattern need be perfect to arrive at a conclusive diagnosis. The method suggests a viable platform that may potentially find use in fault-tolerant and robust point-of-care diagnostic applications.

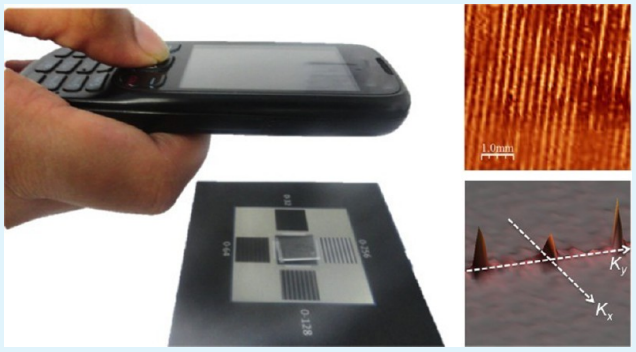

KEYWORDS: *cell phone camera, diagnostics, Fourier transformation, periodically patterned chip, pattern recognition*

INTRODUCTION

Medical diagnostics is continually progressing with the advent of new technologies, such as enzyme-linked immunosorbent assays (ELISA), polymerase chain reaction methodologies (PCR), etc.[1−3] During the last decade, biopatterning leading to biochips gained importance in diagnostics,[4,5] thanks to developments in soft lithography.[6,7] Functionalized micropatterned arrays in the form of stripes or wells, can be created by directly filling with cells,[8] proteins,[9,10] enzymes[11] or DNA,[12] often labelled with fluorophores[13] or biomarkers[14] for optical readout. Such microarrays have been demonstrated for use in a variety of biosensing applications.[15−17] However, for routine usage, a large number of expensive processing steps may prove difficult. In this context, label-free detection using optical diffraction/interference arising directly from the periodic patterns of the printed biochips is promising.[18−20] It relies on the relative change in intensity of the diffracted optical signal following target binding and is shown to be highly specific and sensitive with low detection limits.[21] For accurate detection, however, controlled laboratory environment is required which limits its wide spread applicability. An alternate but nearly equally effective technique would be to replace optical diffraction with fast-Fourier transformation (FFT) of the optical image, as the latter relies on pattern recognition rather than on visual inspection, optical density or number counting.[22,23] Fourier transformation based pattern recognition technique has great potential as non-uniform sizes and orientations of the pathogen do not influence the outcome. For example, Adak et al.[24] have demonstrated sensitive detection of a pathogen, S. aureus, using a dark field microscope to capture the images of patterned arrays, followed by offline FFT processing. If biochip images of the desired quality be obtained using a handy, affordable, and commonly used device the method may potentially become a point-of-care diagnostic technique for low cost settings. In this study, we explore the possibility of using cellphone camera for the purpose due to its affordability and compactness.

Cellphone camera has emerged as a serious imaging tool in medical diagnostic applications.[25−27] For example, Whitesides and co-workers used a microfluidic paper device in conjunction with a cellphone for digital imaging.[28] A compact holographic microscope on a cellphone has been proposed for imaging of microparticles, such as blood cells, platelets, and waterborne parasites.[29] Wide-field fluorescent imaging of white blood cells and protozoan parasites has been demonstrated by incorporating optical components into the existing camera unit.[30]

Received: November 10, 2013
Accepted: February 24, 2014
Published: February 24, 2014

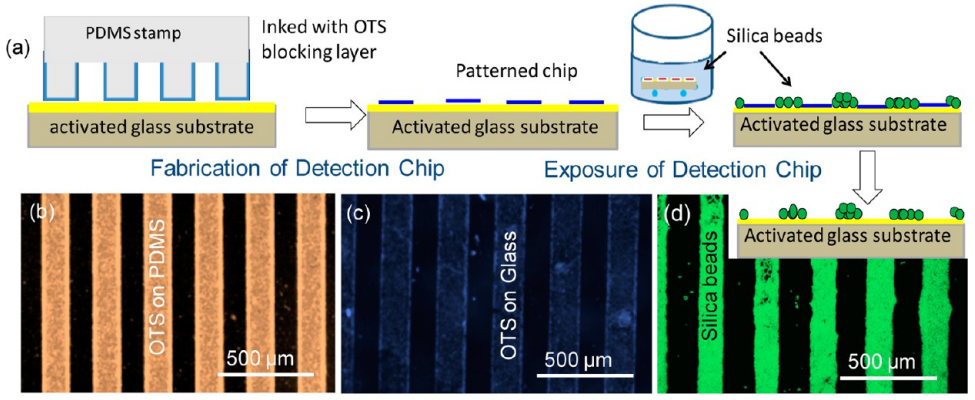

Figure 1. (a) Schematic of the fabrication process of a periodically patterned chip (PPC) on functionalized glass substrate with a blocking layer of OTS molecules. The PPC is exposed to an aqueous dispersion of silica beads used as analyte. Dark-field microscope images of (b) OTS inked on PDMS stamp. (b) OTS after stamping on epoxy functionalized glass substrate. (c) OTS on activated glass substrate. Note that OTS acts like a blocking layer for bead attachment to glass. (d) Silica beads on glass after washing away OTS blocking layer.

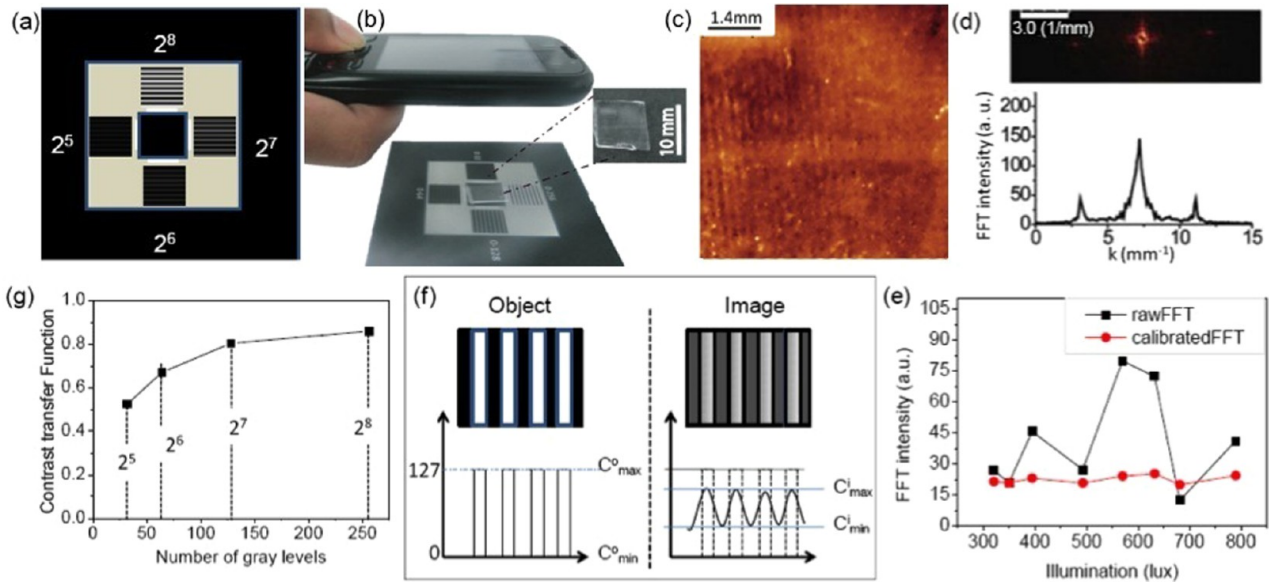

Figure 2. (a) Design of a calibration grid. The square region in the center is for placing the PPC. Sequential steps involved in the image processing of a PPC (exposed to 3 ×10^6 beads/mL solution for 15 min). (b) PPC resting on the calibration grid while a cellphone camera is held approximately horizontal at a suitable distance such that the image occupied the entire screen. The camera was operated in auto focus mode with no flash (luminance, 630 lux). Inset shows the magnified image of PPC along with a scale bar. (c) False-color image selected from a region of the PPC. (d) a 2D image of the Fourier transform along with a line scan positioned to include the Fourier peaks. (e) Raw (black squares) and calibrated (red circles) FFT intensities with respect to variation in luminance. (f) schematic of the calibration pattern used for estimating the contrast transfer function (CTF) of the acquired image. (g) CTF as a function of number of gray scale levels from the calibration grids which was applied on raw FFT to produce calibrated FFT shown in e (red circles). The lines are for guiding the eye.

However, the above examples require extra attachment to a standard cell phone, which anticipates some level of preparedness from the user. It is therefore important to develop methods, which simply rely on the standalone features of the cellphone camera without any attachments. While with progressing technology, the images from a cellphone camera may seem to be FFT worthy, the analysis is notoriously vulnerable to changing lighting conditions during imaging. What is desirable is a patterned chip with built-in calibration, which takes care of the varied light conditions on-field and also be highly defect tolerant. In this report, we demonstrate a method whereby a standard cellphone camera of any make, can produce a digital image acquired under available ambient lighting conditions that provides a quantitative assessment of the concentration of the absorbed microparticles. We devised a simple calibration technique that measures the contrast of a striped pattern, rather than the average intensity of a sample. We have employed micrometer-sized beads of silica (diameter ~5 μm) dispersed in water as analyte to mimic pathogens, a cellphone camera and a Fourier decomposition software on a personal computer to analyse the images. Indeed, the method not only can arrive at a true or false diagnosis but can also provide a quantitative result.

EXPERIMENTAL SECTION

Nexterion-E (epoxy coated) glass slides were purchased from Schott North America (U.S.A.), which are classified as defect-free with high binding efficiency. The periodically patterned chips (PPCs) were obtained on patterning the slides with octadecyltrichlorosilane (OTS) layer by micro-contact printing as described in Supporting Information Figure S1. The periodicity of the pattern was set to 250 μm based on

dx.doi.org/10.1021/am4050426 | ACS Appl. Mater. Interfaces 2014, 6, 3923−3929

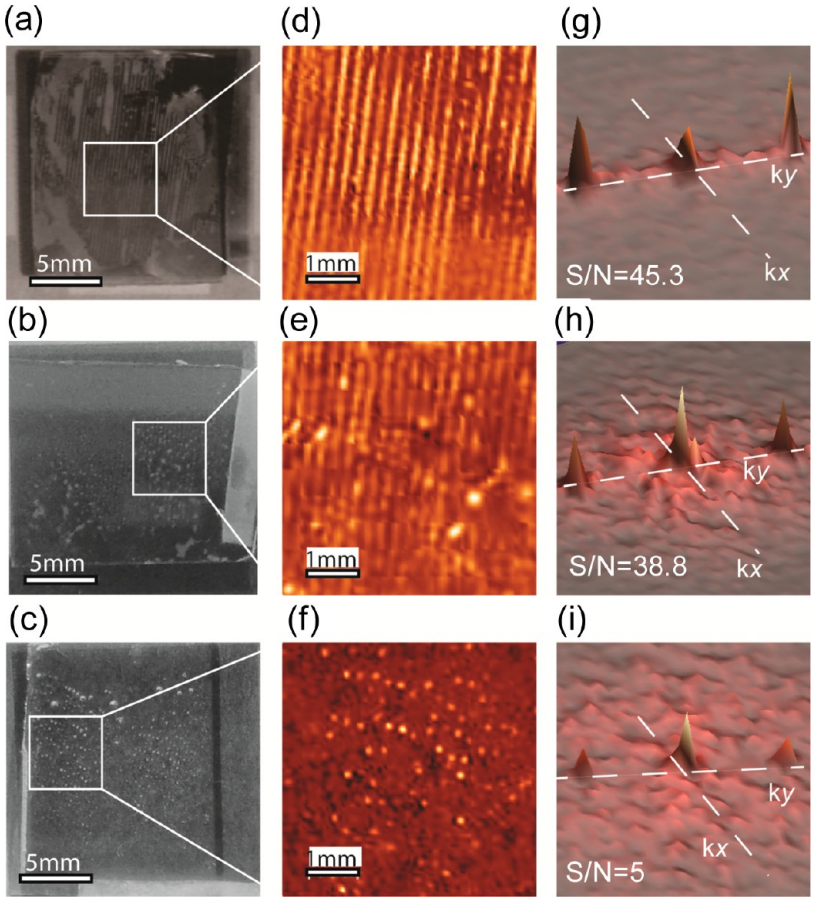

Figure 3. Cellphone camera images of three PPCs exposed to solutions of different concentrations of silica beads for 15 minutes, (a) 10^7, (b) 5×10^6, and (c) 10^5 beads/mL. The corresponding calibrated images d, e, and f and their Fourier maps (g, h, and i) with k_x and k_y axes marked are shown along the rows. The signal to noise ratios are indicated in the Fourier maps.

the resolving capability of a standard 3.2 MP cellphone camera as verified by USAF test pattern (see Supporting Information Figure S2). Dry powder of amine functionalized silica beads (Bangs Laboratories, Inc. SA05N) of diameter 4.63 μm and density of 2 g/cm^3, was used for the study. The beads were dispersed in double distilled water after adding Trixton-X surfactant (20 μL, 0.01 wt%) and sonicating for 20 min to get rid of aggregation. As obtained beads were nearly uniform in size and some clustering was observed (see Supporting Information Figure S3). For exposure of PPC, 5 mL of beads dispersion was used immediately after sonication. After exposing the PPC to the bead dispersion for a preset period of time, the PPC is rinsed to remove the OTS and placed on the central dark square in the middle of the calibration grid. The patterned chips were imaged by cellphone (Nokia-6303c) equipped with a 3.2 MP camera (6.57×10^3 pixels) under constant ambient light illumination using auto-focus with no flash. The other cellphone used in this study was Samsung (Galaxy Note) equipped with a 8 MP (6.75×10^4 pixels) camera. Following the white balance adjustment, the image of the PPC was cropped and calibrated using the scale bar printed on the calibration grid. This formed an image array $f(x,y)$, which was then saved in a black and white TIFF format without compression. In this way, image pixels were accurately converted to lateral dimensions for further analysis by the pattern recognition algorithm (FFT). The integrated intensity of the FFT peak for the first order peak was measured as the readout signal. A 1×1 mm^2 region around each peak was selected and a 'peak-volume' integral was performed to calculate the integrated FFT peak intensity. A brief note on Fourier transformation is given in Supporting Information Note S1.

To estimate the binding efficiency of the beads to the PPC from dispersions of different concentrations, an exposure number was evaluated in each case. Exposure number, denoted by E is defined as the number of bound analytes (beads) per unit area that occur in a unit of time from a given concentration of the bead dispersion. Therefore, a sequence of calibration experiments were performed by exposing unpatterned functionalized Nexterion E slides to solutions of beads with known concentrations (10^5 -10^7 /mL) for different time intervals of 5, 10, and 15 min. The samples were imaged with an inverted dark-field microscope (Laben Instruments, India IM-20BD) equipped with a dark-field condensor and a CCD camera (Pixel Link, PL-S621CU). Automated counting of beads was performed using Image J software. Histograms of the bead count for varying bead concentrations are plotted by analysing 20 different areas of 0.159 mm^2 in each case (see Supporting Information Figure S4). From the exposure analysis, an immersion time of 15 min was chosen for PPC that could detect a concentration between ~10^5–10^7 beads/mL.

RESULTS AND DISCUSSION

In Figure 1a, the PPC fabrication process steps are shown. A PDMS stamp carrying OTS (Figure 1b) was used for microcontact printing on a epoxy coated Nexterion E substrate (Figure 1c), which was dipped in a amine functionalized silica bead dispersion in water (15 min) and then washed in toluene to remove the blocking OTS layer (see Figure 1a). The dark field image in Figure 1d shows high contrast periodic pattern from the adsorbed silica beads. It is clear from the image that the beads are tightly packed in non-blocking areas with negligible non-specific adsorption. The binding efficacy of the Nexterion–E surface is also evident.

Following exposure to analyte dispersion, a PPC was placed on a calibration grid (Figure 2a). The point-of-care condition is

dx.doi.org/10.1021/am4050426 | ACS Appl. Mater. Interfaces 2014, 6, 3923–3929

mimicked by acquiring the image with a hand-held cellphone as shown in Figure 2b. After cropping and linear calibration in WSxM software, the image from a 5 × 5 mm^2 area of the PPC contained typically 4×10^4 pixels. A periodic pattern can be clearly seen in the image due to light scattered by the silica beads that are bound to PPC (Figure 2c). Following FFT (Figure 2d), two first-order bright spots appeared in the 2D Fourier map (Figure 2d) at ±4 mm^{-1} in *k*-space, representing PPC with 250 μm periodicity.

While the positions of the Fourier peaks are predictable, the intensities are subject to imaging conditions, such as shade, sunlight, incandescent, or fluorescent lighting, etc. As shown in Figure 2e, the FFT intensity of the first order peak varied irregularly even under controlled illumination because of built-in camera settings and other external factors. This aspect is duly addressed in this study by white balancing the raw image using disposable paper calibration grid developed for this purpose (see Figure 2a). The calibration grid makes use of contrast transfer function (CTF), which was estimated from sinusoidal contrast patterns containing 2^N gray-scale levels where N = 5, 6, 7, and 8 printed on the calibration grid (see Figures 2a and f). Three of the patterns are used to systematically increase the number of gray scale levels from 2^5 to 2^7, while the fourth pattern spans all 2^8 levels ranging from black (0) to white (255). The maximum contrast for each grid pattern is determined from the digital image while the minimum contrast is set to zero. The white balance in the cellphone camera image of PPC is adjusted by using WSxM software. This adjustment corrects the image, irrespective of the exact lighting conditions. The contrast of the digital image of the calibration grid pattern gives the value of CTF, which is the ratio of the contrast of digital pattern (C_{image}) to the contrast of designed pattern (C_{object}) as shown in Figure 2f. To assess the accuracy of the analysis, it is important to know if the CTF deviated significantly from unity. For white balance correction, the CTF value is estimated by determining the C_{image} and C_{object} for the image in Figure 2c. An analysis of the calibration grid image is depicted in Figure 2g. The CTF value ranges from near unity for an image containing 256 grayscale levels to ∼0.6, for a 32 grayscale image. If the CTF value decreases below ∼0.5, the ability to discern distinct features can become difficult. The raw FFT intensities from PPC images (such as the one shown in Figure 2c) taken under different illuminations were corrected by applying CTF values thus reducing the variation in the FFT signal to below 5% (compare black squares with red circles in Figure 2e).

Following the above procedure, several PPCs were obtained for different concentrations of the bead dispersion and their cellphone camera images were acquired and analyzed (Figure 3). It is significant that the patterns can be easily imaged with a cellphone camera (see Figure 3a−c) under ambient light (∼600 lux). The periodic pattern is clearly visible in the calibrated image for a high concentration of $\sim10^7$ (Figure 3d) as the amount of scattered ambient light is relatively high. Parallely, dark-field microscopy imaging was performed to confirm the observed patterns on the PPC are indeed due to captured beads (see Supporting Information Figure S5). As the bead concentration is reduced, the periodic pattern becomes fainter (see Figure 3e and f). In the FFT maps depicted in Figure 3g−i, the emergence of well-defined peaks at the expected locations in k-space confirms that the binding of the analyte is truly site-specific. Any defects while printing or due to non-specific binding, would broaden the zero-frequency peak centered at k = 0 by distributing intensity throughout the Fourier spectrum. This minimally compromises the signal of interest and produces an inherently fault tolerant approach to analyte detection. Also denoted by S/N ratio, the FFT intensity is found to be 45.3, 38.8, and 5.0 for 10^7, 5×10^6, and 10^5 beads/mL, respectively. When the concentration of beads was below 10^5 beads/mL, the Fourier signal in k-space approached the noise floor setting a lower limit to the concentration that could be measured. Increasing the exposure time for bead adsorption may bring down the limit further (see below).

This suggests that the integrated Fourier signal from an exposed PPC can be used for estimating the unknown concentration of an analyte. In Figure 4, we show how the

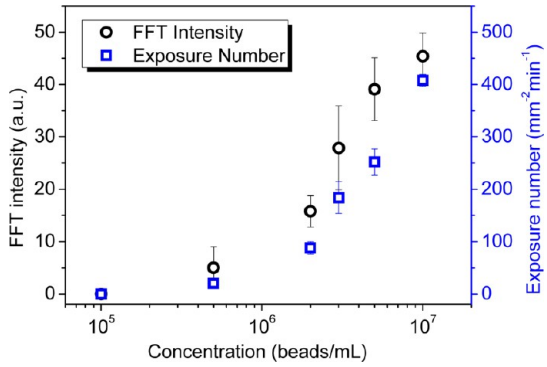

Figure 4. Fourier analysis and exposure number relation with concentration of beads. The integrated Fourier intensity obtained from cellphone camera images of PPCs exposed (left) and exposure number (right) obtained after immersion of functionalized Nexterion E slides to known concentrations of silica beads versus the concentration of the beads.

Fourier intensity signal calculated from a 3.2 MP cellphone camera depends on the concentration of silica beads. Additionally, to substantiate the FFT results, the exposure numbers (defined as number of beads sticking to the pattern per unit area per unit time) were obtained by dipping unpatterned substrates in the bead dispersions of different concentrations. As described under Supporting Information Figure S4, the exposure number is found to vary proportional with time at a given bead concentration which may be taken to indicate that the exposure number obtained for a given dipping time determines the detection range. The good agreement between the two data sets in Figure 4 should provide enough confidence for using a cellphone camera for quantification of adsorbed analyte.

The pattern recognition technique can be extended to sense even lower concentrations of the analyte by either increasing the exposure time or by employing a column summation method described in Figure 5 based on a simulation. Figure 5a shows a simulated image with 256 × 256 pixels where random binding to the substrate is confined to vertical parallel stripes having a periodicity of 12 pixels. This is equivalent to patterning a PPC with vertical stripes of 6 pixel-width where the binding probability is set equal to unity. Outside of the six pixel stripes on either side, the binding probability is set equal to 0. The periodicity may not be evident by visual examination since the number of binding events is rather low, as seen in Figure 5a. On summing the columns across a row, the resulting 1D pattern (Figure 5b) at $k_x = \pm 1/12$ $pixel^{-1}$ showed that the binding is periodic with a known orientation (see enlarged inset). The

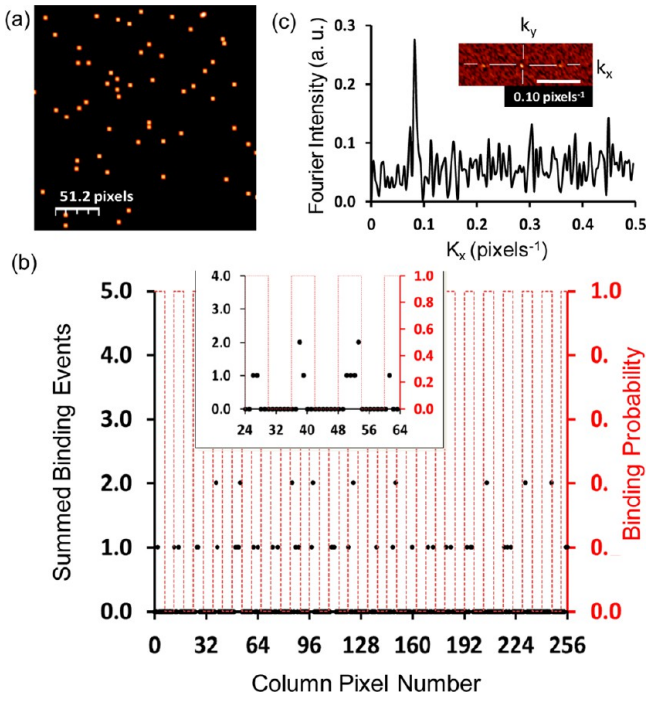

Figure 5. Column summation method for analyte detection at low concentrations. (a) a 256 × 256 pixel simulation with 59 total binding events. (b) The result of summing the binding events in each of the 256 columns. For reference, the modulation of the binding probability is also plotted. (c) 1D Fourier transform of the periodic signal by summing columns. The top inset is a magnified view of a 2D Fourier transform of two peaks at 0.083 pixels^{-1} that are barely visible above the noise floor, providing evidence of periodic binding.

amplified FFT signal in Figures 5c shows a distinct peak at the expected location with a signal to noise ratio of ∼3.

The working range of bead concentration as demonstrated in the above examples need not restrict pathogen detection at lower concentrations in a real scenario. In such instances, beads can be made to serve as carriers for bioanalytes where bead concentration in the dispersion can still be high (∼10^7 beads/mL), while bioanalyte loading on the bead can be much lower (< 10^2/mL). Such concepts have been realised in the literature in optical diffraction studies using beads.[19,20]

We have also examined the effect of the camera resolution in this study (Figure 6). In addition to 3.2 MP cellphone camera (Figure 6a and b), a cellphone with 8 MP camera was used to capture image (Figure 6c) of a given PPC (3 × 10^6 beads/mL, 15 min). The FFT signal was estimated to be 21.22 a.u. for the image captured with 3.2 MP (Figure 6b) and for that from 8 MP camera, 52.86 a.u (Figure 6d). Thus, an equivalent calibration curve for the 8 MP cellphone camera would be 2.5 (= 8/3.2) times the data plotted for 3.2 MP camera as in Figure 4. This analysis shows that the integrated Fourier transform intensity scales roughly with the camera pixels, possibly eliminating the requirement of independent calibration in each case.

Finally, we have validated pattern recognition from cell phone camera images by analysing blood cells in patterns, in place of silica beads. Figure 7a demonstrates the processing steps followed for obtaining such a pattern. The raw blood sample (10 μL) taken from a healthy individual was diluted in DI water (500 μL) and spotted on a PDMS stamp (Figure 7a, left) for direct microcontact printing. The PDMS stamp was

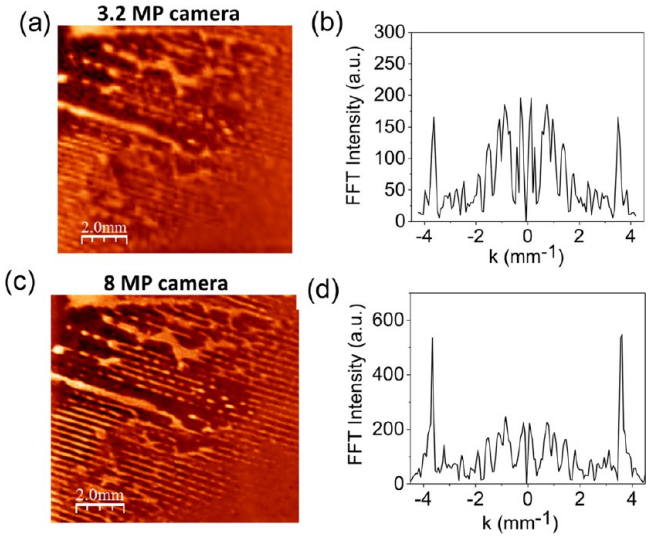

Figure 6. Comparison of cellphone cameras. (a, b) The processed image and its FFT analysis from the image taken by 3.2 MP cellphone camera and (c, d) 8 MP cellphone camera, respectively.

gently pressed against a glass substrate for 2 min and left for drying (Figure 7a, middle). The stamp was removed leaving behind a visually faint blood pattern. As seen from the dark field microscopy images (Figure 7b and c), the patterned regions are filled with blood cells. The pattern could be easily photographed by a 8 MP cellphone camera (see Figure 7d). This clearly shows that the scattering of light from RBCs is good enough to be captured by the cell phone camera similar to the beads used in the earlier part of the study. Fourier transformation of the patterned chip resulted in well-defined spots as seen in the 3D and 2D views with an integrated FFT peak intensity of 68 a.u. (Figure 7e and f, respectively). The image of the control sample without any blood cells in solvent produced zero Fourier amplitude due to the absence of periodic pattern. With the aid of a calibration curve, a meaningful RBC count value may also be possible with this method.

The advantages of the above method using cellphone camera images may be noteworthy. Cellphone with built-in camera, while being widely available and affordable, is a highly standardized tool in terms of technical performance. The fabrication of the periodically patterned chip is based on established procedures in the literature using simple chemical principles. It is important to understand these beads share two important characteristics with bacteria: their size and their ability to reflect visible light. The advantage of this approach is that it allowed us to focus on developing the required steps for a viable pattern recognition method while not being concerned with culturing and handling a particular pathogen. The calibration grids provided around the PPC remove ambiguities with respect to lighting conditions during imaging, which is the main contribution of this work. Pattern recognition using Fourier analysis provides a convenient and unbiased way to analyze periodic pattern without requiring human visual inspection. In addition, the analysis is quantitative. Since Fourier transformation involves a holistic analysis of the selected region of the PPC, neither the pattern nor the substrate need to be uniformly perfect to detect whether a particular analyte is present. The signal of interest (first-order integrated intensity) will result only from the analyte bound to the periodically patterned areas. Defects on the PPC such as

dx.doi.org/10.1021/am4050426 | ACS Appl. Mater. Interfaces 2014, 6, 3923−3929

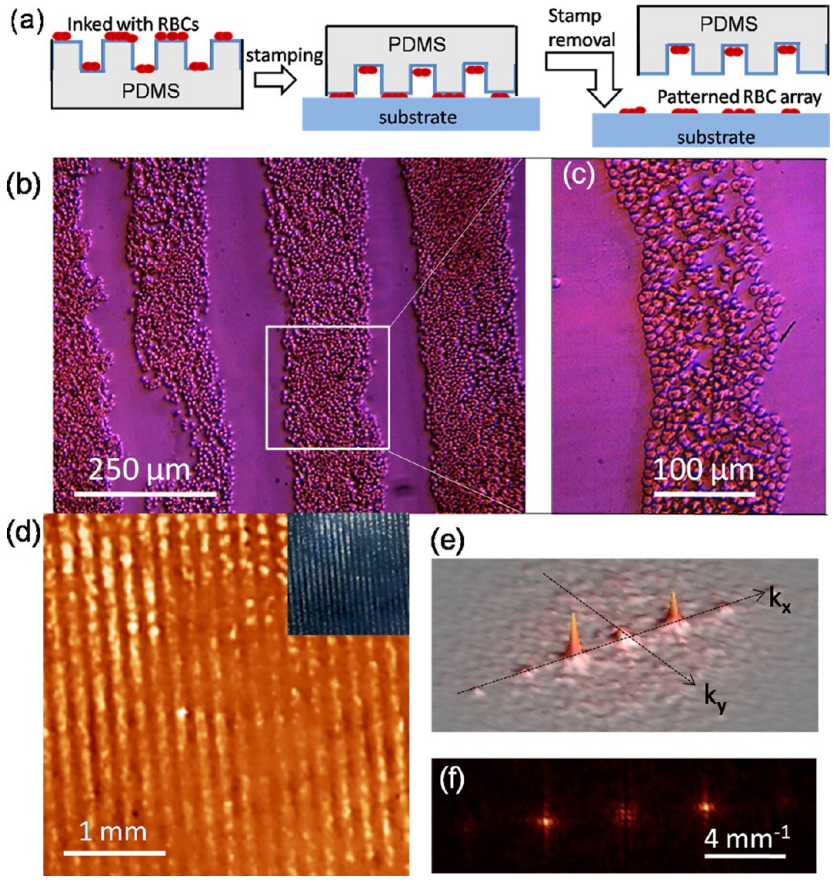

Figure 7. (a) Schematic showing the patterning of red blood cells by micro-contact printing technique. (b) Dark-field microscope image showing the patterned blood cells and (c) in a magnified view. (d) A cellphone camera (8 MP) image zoomed-in to show distinct line patterns filled with red blood cells. The cropped image in its original size (5 mm ×5 mm) is shown in the inset. (e) 3D and (f) 2D views of the Fourier spots obtained from the image.

scratches, dust, imperfections in the printing of the pattern, or non-specific binding at random sites on the chip will contribute to the signal at frequencies other than the characteristic frequencies. Thus, it is an inherently fault-tolerant method that can be applied, in general, to any bio-sensor investigation involving pattern recognition.

CONCLUSIONS

In this study, we have reported a simple pattern recognition method of quantitatively analysing adsorbed microparticles on a periodically patterned chip, which in turn provides an estimate of the microparticle concentration in the dispersion. The pattern recognition is based on Fourier analysis of the chip image taken using standard cellphone camera (3.2 or 8 MP). While the predetermined frequency of the pattern aids Fourier analysis even amidst 'noise' induced by defects thus making the approach fault-tolerant, effects due to varying light conditions during imaging are being taken care by introducing a calibration grid around the chip. The calibration grid consisting of 2^N (N = 5−8) contrast patterns for white balance, enables reliable estimation of the FFT intensity irrespective of the ambient light conditions. The chip consisting of 250 μm periodic lines of octadecyltrichlorosilane (OTS) over 10 × 10 mm^2 area on glass was fabricated using the microcontact printing technique. Silica beads (~5 μm) were used as analyte mimicking bacterial pathogens. The study has given quantitative estimates of analyte concentration in the dispersion in the range, 10^5−10^7 beads/mL. Lower detection limits are possible by increasing the exposure time of the chip in dispersion or as demonstrated by simulation, by 1D summation method in Fourier analysis. Alternatively, the beads can be made to carry bioanalytes adsorbed from solutions of much lower concentrations.

We believe that the study is a step forward in achieving a low cost fault-tolerant technique, which may be extended as a tool for point-of-care diagnostics. The merit of our method lies in its simplicity. Neither our method requires any external optical attachments for quantitative analysis nor do we rely on complicated chemiophysical effects to transduce the signal. The proposed calibration grid can be made downloadable from the internet or saved as an "app" in the cellphone. A brief comparison of our method with existing techniques is made in Supporting Information Table S1.

ASSOCIATED CONTENT

Supporting Information

Figures of experimental description for fabrication of patterned chip and its exposure with silica beads, unprocessed image of the USAF test pattern, determination of exposure number, dark field microscope images on PPC chip after exposure to different concentrations, a brief comparison of present technique with literature methods, and a note on Fourier transform analysis. This material is available free of charge via the Internet at http://pubs.acs.org.

AUTHOR INFORMATION

Corresponding Authors

*E-mail: reifenbr@purdue.edu.

*E-mail: kulkarni@jncasr.ac.in.

Notes

The authors declare no competing financial interest.

ACKNOWLEDGMENTS

We thank Dr. Timothy Fisher, for constant support throughout the project, Dr. Aamer Mahmood for assistance in using clean room facility at Birck Nanotechnology Center, Purdue University. R.G. and G.U.K. thank Prof. C. N. R. Rao for being an inspirational source. R.G.R. is grateful to Profs. P. Low, Y. E. Kim, and A. Wei for helpful discussions throughout this work.

REFERENCES

(1) Pris, A. D.; Mondello, F. J.; Wroczynski, R. J.; Murray, A. J.; Boudries, H.; Surman, C. M.; Paxon, T. L. *Anal. Chem.* **2009**, *81*, 9948−9954.

(2) Clewley, J. P. *The Polymerase Chain Reaction (PCR) for Human Viral Diagnosis*; CRC Press: Boca Raton, FL, 1994.

(3) Costa, J. M.; Pautas, C.; Ernault, P.; Foulet, F. *J. Clin. Microbiol.* **2000**, *38*, 2929.

(4) Grow, A. E.; Wood, L. L.; Claycomb, J. L. *J. Microbiol. Methods* **2003**, *53*, 221.

(5) Mir, M.; Dondapati, S. K.; Duarte, M. V. *Biosens. Bioelectron.* **2010**, *25*, 2115.

(6) Qin, D.; Xia, Y.; Whitesides, G. M. *Nat. Protoc.* **2010**, *5*, 491.

(7) Michel, B.; Bernard, A.; Bietsch, A.; Delamarche, E.; Geissler, M.; Juncker, D.; Kind, H.; Renault, J. P.; Rothuizen, H.; Schmid, H.; Schmidt-Winkel, P.; Stutz, R.; Wolf, H. *IBM J. Res. Dev.* **2001**, *45*, 697.

(8) Bai, H.-J.; Shao, M.-L.; Gou, H.-L.; Xu, J.-J.; Chen, H.-Y. *Langmuir* **2009**, *25*, 10402−10407.

(9) Kane, R. S.; Takayama, S.; Ostuni, E.; Ingber, D. E. *Biomaterials* **1999**, *20*, 2363.

(10) Qin, D.; Xia, Y.; Whitesides, G. M. *Nat. Protoc.* **2010**, *5*, 491.

(11) Mugherli, L.; Burchak, O. N.; Balakireva, L. A.; Thomas, A.; Chatelain, F.; Balakirev, M. Y. *Angew. Chem.* **2009**, *121*, 7775.

(12) Schumacher, A.; Weinhäusl, A.; Petronis, A. *Methods Mol Biol* **2007**, *439*, 109.

(13) Chen, L.Y.; Huang, C. C.; Chen, W.-Y.; Lin, H.-J.; Chang, H.T. *Biosens. Bioelectron.* **2013**, *43*, 38.

(14) Jordan, B. *Microarrays in Diagnostics and Biomarker Development*; Springer: Heidelberg, Germany, 2012.

(15) Stratis-Cullum, D. N.; Griffin, G. D.; Mobley, J.; Vass, A. A.; Vo-Dinh, T. *Anal. Chem.* **2003**, *75*, 275.

(16) Abbas, A.; Linman, M. J.; Cheng, Q. *Anal. Chem.* **2011**, *83*, 3147.

(17) Ruiz, A.; Buzanska, L.; Gilliland, D.; Rauscher, H.; Sirghi, L.; Sobanski, T.; Zychowicz, M.; Ceriotti, L.; Bretagnol, F.; Coecke, S.; Colpo, P.; Rossi, F. *Biomaterials* **2008**, *29*, 4766.

(18) Chang, C. L.; Acharya, G.; Savran, C. A. *Appl. Phys. Lett.* **2007**, *90*, No. 233901.

(19) Acharya, G.; Chang, C.-L.; Doorneweerd, D. D.; Vlashi, E.; Henne, W. A.; Hartmann, L. C.; Low, P. S.; Savran, C. A. *J. Am. Chem. Soc.* **2007**, *129*, 15824.

(20) Acharya, G.; Chang, C.-L.; Holland, D. P.; Thompson, D. H.; Savran, C. A. *Angew. Chem., Int. Ed.* **2007**, *47*, 1051.

(21) Acharya, G.; Doorneweerd, D. D.; Chang, C.-L.; Henne, W. A.; Low, P. S.; Savran, C. A. *J. Am. Chem. Soc.* **2007**, *129*, 732.

(22) Kim, Y.; Lyvers, D. P.; Wei, A.; Reifenberger, R. G.; Low, P. S. *Lab Chip* **2012**, *12*, 971.

(23) Doorneweerd, D. D.; Henne, W. A.; Reifenberger, R. G.; Low, P. S. *Langmuir* **2010**, *26*, 15424.

(24) Adak, A. K.; Boley, J. W.; Lyvers, D. P.; Chiu, G. T.; Low, P. S.; Reifenberger, R.; Wei, A. *ACS Appl. Mater. Interfaces* **2013**, *5*, 6404.

(25) Wei, Q.; Qi, H.; Luo, W.; Tseng, D.; Ki, S. J.; Wan, Z.; Göröcs, Z.; Bentolila, L. A.; Wu, T.-T.; Sun, R.; Ozcan, A. *ACS Nano* **2013**, *7*, 9147.

(26) Breslauer, D. N.; Maamari, R. N.; Switz, N. A.; Lam, W. A.; Fletcher, D. A. *PLoS ONE* **2009**, *4*, No. e6320.

(27) Tuijn, C. J.; Hoefman, B. J.; van Beijma, H.; Oskam, L.; Chevrollier, N. *PLoS ONE* **2011**, *6*, e28348.

(28) Martinez, A. W.; Phillips, S. T.; Carrilho, E.; Thomas, S. W.; Sindi, H.; Whitesides, G. M. *Anal. Chem.* **2008**, *80*, 3699.

(29) Zhu, H.; Yaglidere, O.; Su, T.-W.; Tseng, D.; Ozcan, A. *Lab Chip* **2011**, *11*, 315.

(30) Zhu, H.; Sikora, U.; Ozcan, A. *Analyst* **2012**, *137*, 2541.